Surface Chemistry |*Hot Paper*|

The Macrocycle versus Chain Competition in On-Surface Polymerization: Insights from Reactions of 1,3-Dibromoazulene on Cu(111)

Claudio K. Krug[+],[a] Damian Nieckarz[+],[b] Qitang Fan,[a] Paweł Szabelski,[b] and J. Michael Gottfried*[a]

Abstract: Ring/chain competition in oligomerization reactions represents a long-standing topic of synthetic chemistry and was treated extensively for solution reactions but is not well-understood for the two-dimensional confinement of surface reactions. Here, the kinetic and thermodynamic principles of ring/chain competition in on-surface synthesis are addressed by scanning tunneling microscopy, X-ray photoelectron spectroscopy, and Monte Carlo simulations applied to azulene-based organometallic oligomers on Cu(111). Analysis of experiments and simulations reveals how the ring/chain ratio can be controlled through variation of coverage and temperature. At room temperature, non-equilibrium conditions prevail and kinetic control leads to preferential formation of the entropically favored chains. In contrast, high-temperature equilibrium conditions are associated with thermodynamic control, resulting in increased yields of the energetically favored rings. The optimum conditions for ring formation include the lowest possible temperature within the regime of thermodynamic control and a low coverage. The general implications are discussed and compared to the solution case.

Introduction

The competition between chain and ring formation in polymerization reactions has been a long-standing topic in synthetic chemistry[1–4] and has recently also found attention in on-surface synthesis.[5–9] The polymerizations can be performed under equilibrium or non-equilibrium conditions. Equilibrium implies that the decisive bonds are reversibly formed and dissociated during the reaction. These conditions lead to thermodynamic reaction control, which means that the product composition is determined by the relative thermodynamic stabilities, that is, by the standard free enthalpy of the reaction. In contrast, non-equilibrium conditions result in kinetic reaction control. In the limiting case that the rate of the backwards reaction is zero, the product composition is exclusively controlled by the relative rates of formation of the different products. The equilibrium case for oligomerization reactions in three-dimensional (3D) solution phases was first treated by Jacobson and Stockmayer using flight statistics,[1] an approach that was later refined.[10] In contrast, systems under kinetic control proved to be more difficult to describe.[2] Eventually, it was shown that the ring-size distribution under kinetic control is similar to that predicted for equilibrium conditions by the Jacobson–Stockmayer model.[3]

In on-surface polymerizations, the product composition is additionally influenced by the two-dimensional (2D) confinement and the specific interactions of the reactants with the surface. As a model reaction related to on-surface synthesis of carbon-based nanostructures,[11–22] we study here the formation of azulene-based organometallic oligo- and polymers from 1,3-dibromoazulene (DBAz, Figure 1). Such organometallic compounds of aromatic building blocks represent important and stable intermediates in the Ullmann-type on-surface synthesis of carbon-based nanostructures.[5,23] Previous work has shown that the linking pattern in the organometallic intermediates determines the structure of the covalent end product of the surface Ullmann coupling.[6] Therefore, it is important to control the structures of these intermediates.

Azulene is a building block with a prototypical non-alternant aromatic π-electron system, which has recently attracted attention in surface chemistry, organic electronics, and related areas.[24–35] Non-alternant aromatic π-electron systems typically

[a] C. K. Krug,[+] Dr. Q. Fan, Prof. Dr. J. M. Gottfried
Department of Chemistry, Philipps University Marburg
Hans-Meerwein-Straße 4, 35032 Marburg (Germany)
E-mail: michael.gottfried@chemie.uni-marburg.de

[b] Dr. D. Nieckarz,[+] Prof. Dr. P. Szabelski
Department of Theoretical Chemistry, Institute of Chemical Sciences
Faculty of Chemistry, Maria Curie-Skłodowska University in Lublin
Pl. M.C. Skłodowskiej 3, Lublin 20-031 (Poland)

[+] These authors contributed equally to this work.

Supporting information and the ORCID identification number(s) for the author(s) of this article can be found under: https://doi.org/10.1002/chem.202000486.

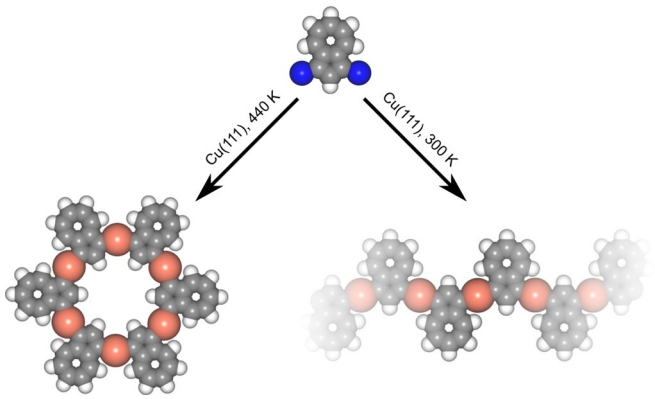

Figure 1. Space-filling model showing the possible cyclic (left) and open-chain (right) organometallic reaction products of 1,3-dibromoazulene (DBAz) on Cu(111). The ring/chain competition under kinetic and thermodynamic control is analyzed in this work. Color code: white, hydrogen; grey, carbon; red, copper; blue, bromine.

contain odd-numbered rings such as pentagons and heptagons. Their electronic properties differ strongly from those of their alternant isomers, resulting in stronger interactions with metal surfaces.[34] Non-alternant structural motifs also occur as defects in graphene and carbon nanotubes and influence their properties.[36–39]

In this work, we study the ring/chain competition in two-dimensional (2D) confinement using azulene-based organometallic oligomers. As was shown in a preliminary Communication,[9] the dominant cyclic product is the hexamer shown in Figure 1 (left) and the ring/chain competition can be influenced by reaction temperature and coverage. Here, we provide a comprehensive treatment of the observed phenomena in the context of thermodynamic and kinetic reaction control, using Monte Carlo (MC) simulations for the interpretation of the experimental data obtained by analysis of scanning tunneling microscopy (STM) images. In addition, we apply the concept of the effective molarity (EM) for the first time to on-surface chemistry.

Results and Discussion

Non-equilibrium conditions and kinetic reaction control

Figure 2 shows STM images taken after the deposition of 1,3-dibromoazulene (DBAz) on Cu(111) at 300 K, using four different coverages. At this temperature, the C–Br bonds dissociate, as was confirmed by XPS (see Figure S1 in the Supporting Information). The resulting debrominated azulene units form organometallic oligomers with C-Cu-C bonds, as shown in Figure 1.[9] According to previous work, the C–Cu bond is stable over the duration of the experiment at 300 K.[7,40–42] Therefore, we have a non-equilibrium situation of kinetic reaction control, which means that the initially formed product (i.e., the species that is produced with the fastest rate) prevails.

Statistically, the formation of chains is expected to be favored under these conditions, because there are more conformers (i.e., possible realizations) for an *n*-membered chain

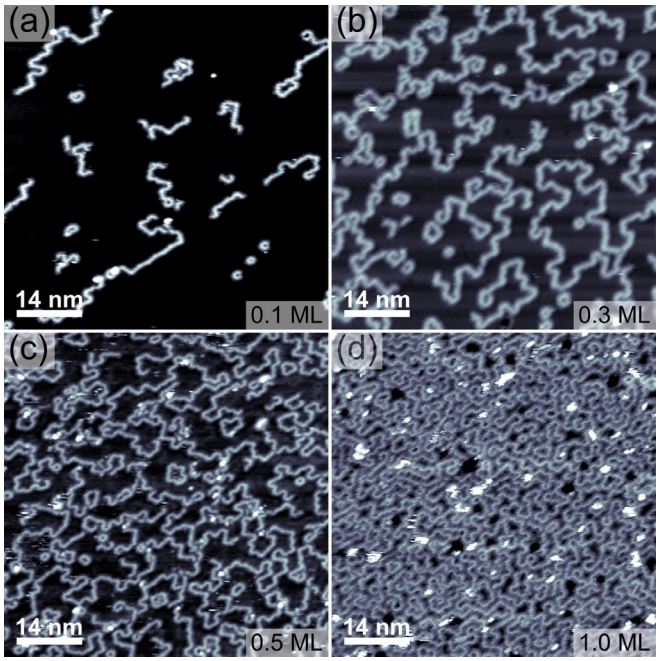

Figure 2. STM images of DBAz on Cu(111) after deposition at 300 K for four different coverages as indicated in the images. Tunneling parameters: (a) $U=-3.52$ V, $I=-0.09$ nA; (b) $U=-1.74$ V, $I=-0.15$ nA; (c) $U=-3.63$ V, $I=-0.16$ nA; (d) $U=-1.85$ V, $I=-0.11$ nA.

compared to an *n*-membered ring.[9] A small *n*-membered ring, such as the hexamer in Figure 1 with $n=6$, requires *cis*-configuration of all azulene units. Since an individual unit is *cis*-oriented relative to an existing segment with a probability of 0.5, the total probability for the formation of an *n*-membered ring is 0.5^{n-1}. All other, mixed *cis*/*trans* configurations with *n* segments can only form chains and therefore have a total combined probability of $1–0.5^{n-1}$. In the case of $n=6$, the probability for the formation of a hexamer under kinetic control is therefore only 1/32. Noteworthy, larger macrocycles may contain segments with *trans*-oriented units, which leads to a more complex situation.

Another important factor that controls the ring/chain ratio is the coverage, because the ring closure and the chain growth have different reaction orders and thus the ratio of their rates is coverage-dependent.[6,9] Generally, the intramolecular ring closure as a first-order reaction (Equation 1) with the rate constant k_{intra} prevails at low precursor coverage, while the chain growth as an intermolecular second-order reaction (Equation 2) with the rate constant k_{inter} will increasingly compete when the coverage is increased.[6]

$$M_6 \xrightarrow{k_{intra}} C_6 \quad (1)$$

$$M_i + M_1 \xrightarrow{k_{inter}} M_{i+1} \quad (2)$$

Based on these considerations, the STM data in Figure 2 can be understood qualitatively. In the following, we will discuss the relative yield of rings, especially of the dominant cyclic hexamers. This yield is defined as the percentage of monomer units incorporated in the cyclic hexamers.

Analysis for the sample with the lowest coverage (0.1 ML, Figure 2a) reveals that only 3% of the monomer units are incorporated in cyclic hexamers, close to the statistically expected value of $0.5^5 = 3.125\%$.[9] Increasing the coverage to 0.3 and 0.5 ML (Figure 2b,c) reduces the yield of rings to 2%. For the saturation coverage at 300 K (Figure 2d, coverage defined as 1.0 ML), the yield is even lower with 1%. Thus, the data show the expected trend of lower ring yields at higher coverages.

In homogeneous reactions (gas phase or solution), one advantage of ring closure over chain growth arises from the fact that the latter requires the bond formation between two reactants. As a result, three degrees of translational freedom and three degrees of rotational freedom of the two reactants are converted into six new degrees of vibrational freedom of the product, lowering its entropy content. Accordingly, ring formation can be entropically favored over chain formation.[43] In the adsorbed state, however, these translational and rotational degrees of freedom of the reactants are already mostly frustrated, that is, converted to vibrations. The loss of entropy content during chain formation is therefore expected to be much smaller. The situation may even be reversed, because the open radical ends of the reactants are expected to bind more strongly to the surface, and thus have less degrees of translational and rotational freedom than the product they form.

Equilibrium conditions and thermodynamic reaction control

The four different samples from Figure 2 were annealed to 440 K for 5 minutes and then cooled rapidly to the imaging temperature of 100 K. The temperature of 440 K was chosen to ensure chemical equilibrium, that is, fast reversible formation and dissociation of the organometallic C–Cu bonds. This reversible character of the C–Cu bonds at elevated temperatures at and above 440 K is well established.[5,44] Under these conditions, the product composition is given by the equilibrium constant and thus reflects the thermodynamic stability of the products. As shown by the STM images in Figure 3, now the cyclic hexamers are formed with much higher yields, indicating that they represent the thermodynamically more stable product.[9]

For the low-coverage sample (0.1 ML, Figure 3a), the ring yield is increased from 3% under kinetic control to 78% under thermodynamic control. For the samples with coverages of 0.3 and 0.5 ML (Figure 3b,c and Figure S2 in the Supporting Information) the ring yields are now 22 and 17%, respectively, which is also significantly increased compared to kinetic control. At 1.0 ML, large lateral fluctuations of the local concentration of rings are observed (Figures 3d and 3e). Apparently, the rings are sufficiently mobile at 440 K to aggregate into large islands, as shown in Figure 3e. These islands are stabilized by the interaction with the split-off Br atoms, which can be seen in Figure S3g,h in the Supporting Information.[5,45] In Figure 3f, the ring yields are plotted as functions of the coverage, illustrating that thermodynamic control leads to much higher ring yields than kinetic control.

Enlarged images of islands of hexamers are displayed in Figure 4 and Figures S3 and S4 in the Supporting Information. The images in Figures 4a and 4b were taken at different tunneling conditions. In Figure 4a, the Cu atoms appear as protrusions, whereas Figure 4b also shows the azulene units as bright uniform features. Related images of the chains at differ-

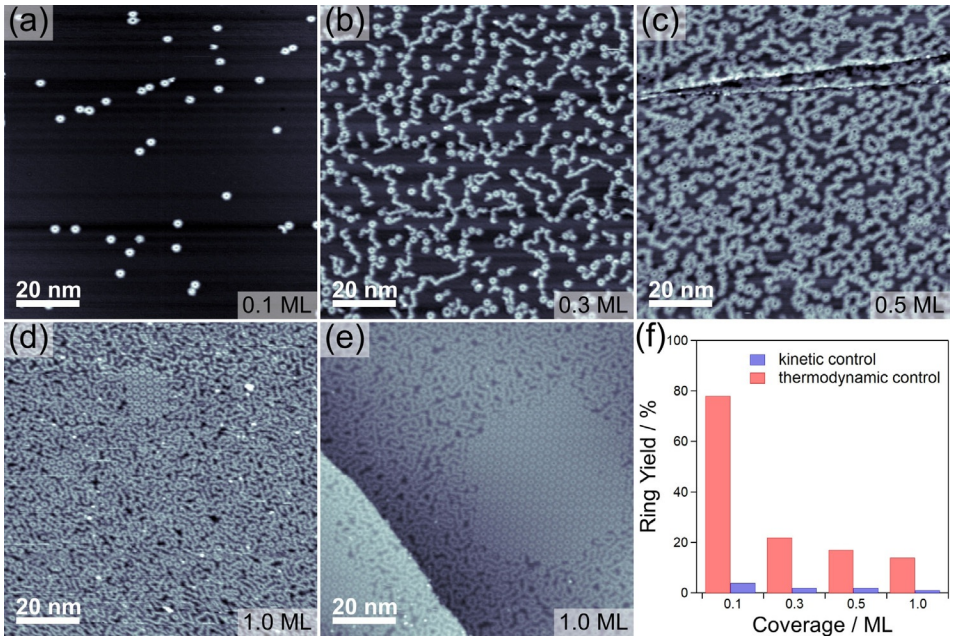

Figure 3. (a)–(e) STM images of DBAz on Cu(111) after annealing the four samples shown in Figure 2 to 440 K. Coverages as indicated in the images. For 1.0 ML, two different sample regions are shown. (f) Relative yield of hexamer rings as a function of the total coverage at 300 K (kinetic control) and 440 K (thermodynamic control). The percentage of rings (ring yield) is defined here as the total number of repeat units contained in cyclic hexamers divided by the total number of repeat units contained in chains and rings. Tunneling parameters: (a) $U = -2.84$ V, $I = -0.13$ nA; (b) $U = -1.10$ V, $I = -0.12$ nA; (c) $U = -3.52$ V, $I = -0.19$ nA; (d) $U = -3.63$ V, $I = -0.10$ nA; (e) $U = -3.31$ V, $I = -0.11$ nA.

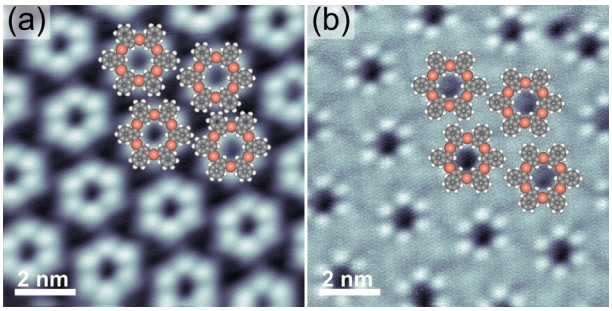

Figure 4. STM images of an island of the cyclic hexamer macrocycles, taken at different tunneling conditions, with overlaid molecular models. In image (a), the bridging Cu atoms are shown as bright protrusions, whereas (b) also shows the azulene units as bright features. Tunneling parameters: (a) $U=-0.94$ V, $I=-0.10$ nA; (b) $U=1.79$ V, $I=0.10$ nA.

ent tunneling conditions are shown in Figure S5 in the Supporting Information.

The formation of cyclic hexamers is remarkable, because they are strained, while the structure of the azulene molecule should enable the formation of strain-free cyclic decamers. The predominant formation of hexamers is attributed to registry effects. Azulene adsorbed on Cu(111) prefers adsorption sites on which the long molecular axis is aligned along a high-symmetry direction of the surface,[34] resulting in six possible preferential orientations. In the cyclic hexamer, all azulene units can assume their preferred orientation, while this is not the case for the cyclic decamer. The latter, although unstrained, is therefore energetically unfavorable. In rare cases, cyclic octamers were observed (see Figure S6 in the Supporting Information).

The variation of the ring yield with coverage (Figure 3 f) reflects the dynamic character of the chemical equilibrium between rings and chains. As mentioned above, the ring closure and chain growth have different reaction orders. With increasing coverage, the rate of the second-order chain growth increases faster than that of the first-order ring closure. As a result, the equilibrium is shifted towards the side of the chains as the coverage increases. (This trend is also reproduced by the MC simulations, as shown below and in Figure S10 in the Supporting Information)

The very high ring yield observed at the lowest coverage (see Figure 3 a and Figure S7 in the Supporting Information) is reminiscent of a specific result of the Jacobson–Stockmayer (J–S) theory. It predicts the existence of a critical concentration, below which the system consists entirely of rings.[1] However, the J–S theory was derived for rings that are sufficiently large to avoid short-range steric effects. Only then, the probability of the ring closure can be expressed as a well-defined function of the ring size. Here, we consider a 2D system, in which the molecules are confined to certain lattice sites. This confinement influences both the energy and the entropy term of the reaction free enthalpy (see below). The effects of the 2D confinement on the energy include the adsorbate–surface interaction energy and steric strain resulting from a forced planar geometry. The entropy term is influenced by excluding all non-planar conformations. Especially in the case of chains, which have a larger number of non-planar conformations than the rings, the 2D confinement should substantially reduce their entropy. The small size and the strained structure of the cyclic hexamers, along with effects of the 2D confinement, therefore limit the applicability of the J–S model for 2D systems, as was also previously observed.[6] As a consequence, we resorted to MC simulations to gain further insight into the different types of reaction control.

Monte Carlo simulations

In the MC model shown in Figure 5, the triangular lattice of equivalent adsorption sites represents a highly symmetric (111) surface, such as Cu(111). The azulene units are abstractly modelled as two planar, interconnected segments with an active part (red) and an inactive part (grey). One segment can occupy one adsorption site on the lattice, as is experimentally justified, because the azulene molecules show a strong adsorption site preference with alignment of the long molecular axis parallel to the high-symmetry directions of the Cu(111) surface.[34] The bonds between the model molecules are directional and limited to neighboring adsorption sites on the lattice. The molecules interact with the energy $\varepsilon=-1.0$. All remaining interactions, including the molecule-molecule and molecule-surface interactions, are neglected. The MC simulations were carried out in the canonical ensemble, where the number of molecules N, the size of the system L, and the temperature T were constant.[46,47] For further details, see the Experimental and Computational Details section.

Figure 6 shows the results of the MC simulations for low-temperature non-equilibrium conditions (Figures 6 a and 6 c, kinetic reaction control) in comparison with the high-temperature equilibrium conditions (Figures 6 b and 6 d, thermodynamic reaction control). The ratio of the two temperatures is the same as in the experiment (440 K, 300 K) with $T_{high}/T_{low}=1.47$. At low coverage under kinetic control (Figure 6 a), a considerable number of chains is formed, whereas cyclic hexamers dominate under thermodynamic control (Figure 6 b). Comparison of the simulated with the corresponding experimental

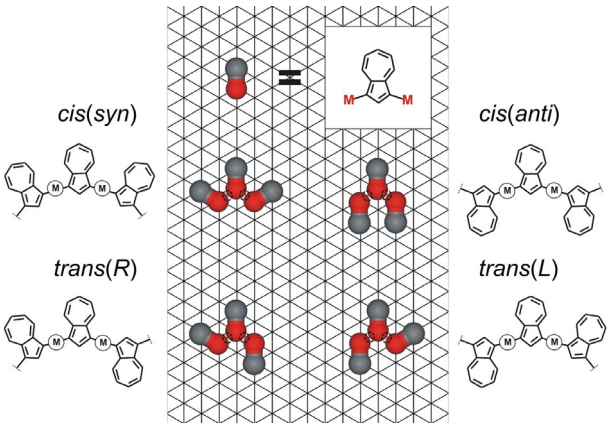

Figure 5. Model for the MC simulations. The azulene units are abstractly modeled as planar, interconnected segments with an active part (red) and an inactive part (grey). Four different connection motifs of three units are shown.

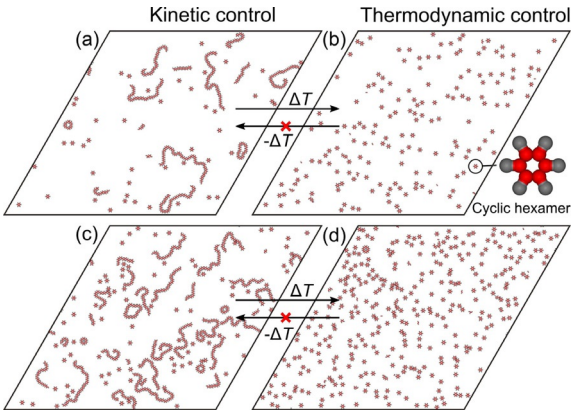

Figure 6. MC simulations with the model in Figure 5 for two different coverages ((a), (b) 0.05, and (c), (d) 0.1) and two different temperatures. The temperatures have a ratio of $T_{high}/T_{low} = 1.47$, which is identical to the experimental ratio. (a), (c) Low temperature, non-equilibrium conditions, kinetic control. (b), (d) High temperature, equilibrium conditions, thermodynamic control. The arrows between (a) and (b) as well as (c) and (d) express that it is possible to shift the systems from the non-equilibrium to the equilibrium state by increasing the temperature, whereas it is not possible to go the reverse way by lowering the temperature.

data (e.g., Figure 2a vs. Figure 6a and Figure 3a vs. Figure 6b) reveals a good qualitative agreement, which is quite remarkable considering the high degree of abstraction in the model system. It shows that the model captures important features of the system, in particular the transformation from kinetic to thermodynamic control, and that these features have a high degree of commonality.

Doubling the coverage (Figures 6c and 6d) leads to qualitatively similar results: At low temperature (Figure 6c), the formation of chains prevails, whereas high-temperature conditions lead to the formation of mostly hexamer macrocycles (Figure 6d). In the simulations, sometimes larger rings than cyclic hexamers are observed. An experimental example is shown in Figure S8 in the Supporting Information. Further MC simulations for two additional coverages are shown in the Supporting Information, Figures S11 and S12.

Figure 7 compares the relative abundances (fractions) of the four different main structural motifs, as defined in Figure 7a. The color code in Figure 7a corresponds to the colors in the bar graphs in Figures 7b–7g. The *cis*(*syn*) motif (red) is the only motif that occurs in the cyclic hexamers, while it rarely occurs in chains. All other motifs, that is, *cis*(*anti*), *trans*(*R*) and *trans*(*L*), occur only in chains. Therefore, the abundance of the *cis*(*syn*) (red), compared to the abundances of the other motifs, is a good approximation for the ratio of rings versus chains.

The data in Figure 7 reveal that the transition from kinetic to thermodynamic control leads to an increased formation of the *cis*(*syn*) motif. At the lowest coverage (Figures 7b and 7e), this change is very substantial, as the fraction of *cis*(*syn*) increases from 0.32 to 0.98.

The coverage-dependent changes in the regime of thermodynamic control (*cf.* Figures 7e–7g) reveal that the macrocycles are less favored at higher coverages. The same trend was observed experimentally (*cf.* Figure 3f) and was explained

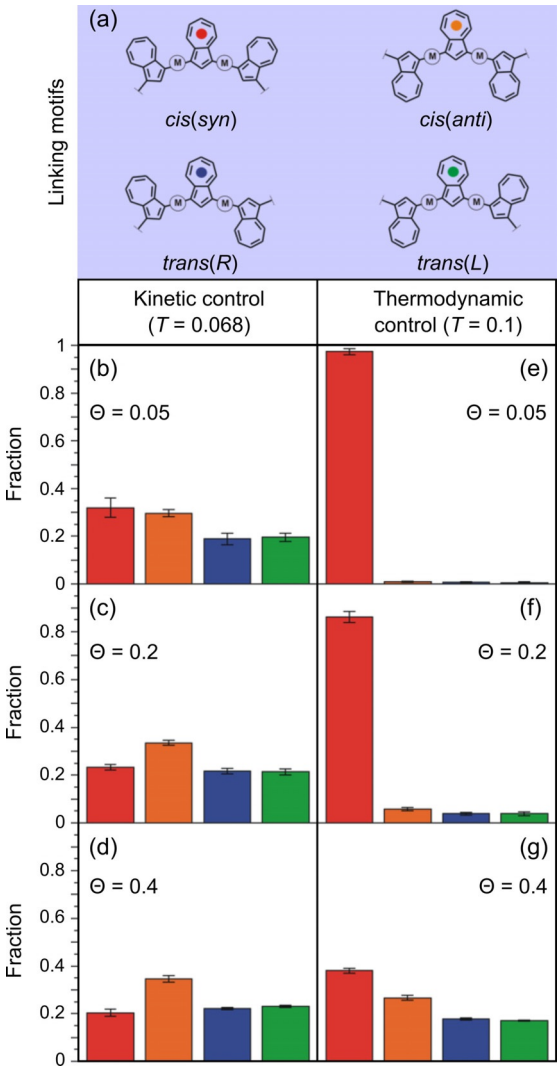

Figure 7. Relative abundances (fractions) of the main structural linking motifs defined in (a), obtained from the MC simulations for different coverages and temperatures. The presented results are averages from 10 independent systems. (b)–(d) Low temperature, kinetic control; (e)–(g) high temperature, thermodynamic control. The colors in the bar graphs correspond to the color scheme defined in (a).

above by the different reaction orders for ring and chain formation. The fact that the rather abstract MC model describes these trends correctly indicates that the ring/chain ratio is indeed largely controlled by fundamental principles, rather than specific properties of our system. Complete quantitative agreement for the abundances for the different structural motifs in experiment and simulation cannot be expected, because the equilibrium is additionally influenced by factors neglected in the MC simulations, especially molecular structure, specific interaction with the surface, or intermolecular interactions.

In the regime of kinetic control, similar coverage-dependent trends are observed (Figures 7b–7d). With increasing coverage, the fraction of the ring-related *cis*(*syn*) motif decreases. In contrast, the fractions of the other motifs increase, especially that of the *cis*(*anti*) motif (orange), which occurs in straight chain

segments. The same trend was observed in the experiment (*cf.* Figure 2 and Figure 3 f).

Optimal reaction temperature for ring formation

Above, we have shown by experiment and simulation that the ring yield under thermodynamic control depends on the coverage of azulene monomers. Now, we focus on the influence of the temperature and determine, whether there is an optimal temperature, at which the ring yield reaches its maximum. For this aim, an intermediate coverage of 0.5 ML of DBAz was deposited on Cu(111) at 300 K. Thereafter, the sample was stepwise annealed for 5 minutes, followed by rapid cooling to the imaging temperature of 100 K (Figure 8).

Deposition of DBAz at 300 K leads to predominant chain formation and a low ring yield (3%, Figure 8 a), in agreement with the result discussed above for kinetic control. Annealing this sample to 350 K does not increase the ring yield (Figure 8 b). Apparently, this temperature is still within the regime of kinetic control. It requires annealing to 390 K to observe a slight increase of the ring yield to 8% (Figure 8 c). The maximum ring yield of 20% is obtained after annealing at 430 K (Figure 8 d). This value is slightly higher than that obtained after annealing a different sample with the same coverage to 440 K (*cf.* Figure 3 c, 17%). If the sample is annealed to 460 K (Figure 8 e and Figure S9 in the Supporting Information), the trend is reversed and a decrease in the ring yield to 18% is observed. Further annealing to 470 K (Figure 8 f) is accompanied by the onset of desorption. As a result, the residual coverage is reduced to 0.4 ML, while the ring yield remains at 18%. The temperature dependence of the ring yield is summarized in Figure 9 a.

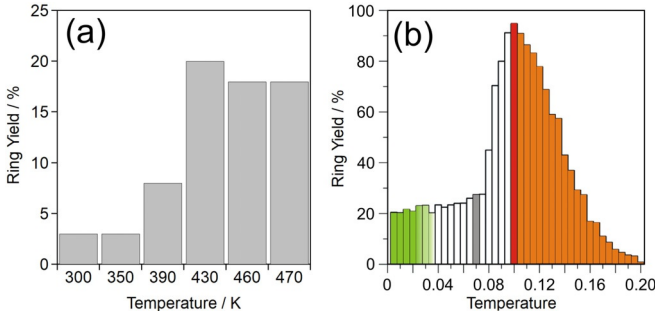

Figure 9. (a) Yield of hexamer rings as a function of temperature, as derived from the STM images in Figure 8. (b) Percentage of molecules contained in hexamer rings in the MC simulations as a function of temperature (for a coverage of 0.05). The green bars indicate temperatures at which on-surface diffusion of the molecules is very slow. Bars marked in orange correspond to high temperatures, at which competing processes such as desorption or degradation are significant in experimental systems.

Monte Carlo simulations

The MC simulations (Figure 9 b) showed that the yield of hexagonal rings has a maximum at an intermediate temperature, in qualitative agreement with the experimental data. The existence of an optimal temperature for macrocycle formation can be understood based on the principles introduced above: At low temperatures, kinetic control favors chain formation at the expense of ring formation. This explains the low ring yields in the low-temperature range.

The decreasing ring yields at high temperatures, that is, under thermodynamic control, require a thermodynamic argument based on the standard free enthalpy $\Delta G^\circ = \Delta H^\circ - T\Delta S^\circ$, which determines the ring/chain equilibrium. (ΔH° *is* the stan-

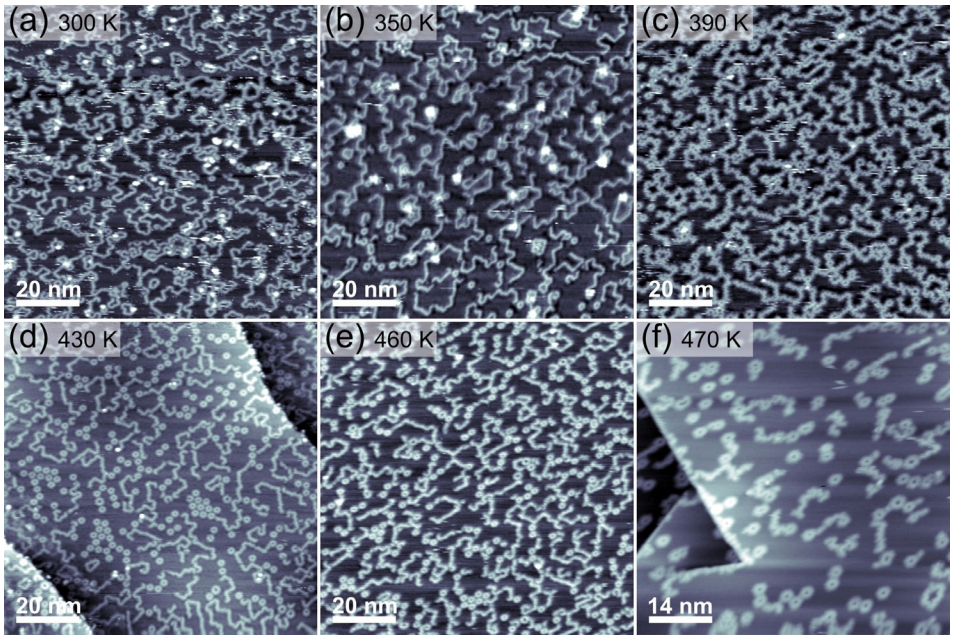

Figure 8. STM images of 0.5 ML DBAz on Cu(111) after deposition at 300 K and annealing (5 minutes) to the indicated temperatures, followed by rapid cooling to 100 K for imaging. Tunneling parameters: (a) $U = -3.63$ V, $I = -0.14$ nA; (b) $U = -3.63$ V, $I = -0.13$ nA; (c) $U = -3.63$ V, $I = -0.14$ nA; (d) $U = -3.63$ V, $I = -0.10$ nA; (e) $U = -3.63$ V, $I = -0.11$ nA; (f) $U = -3.63$ V, $I = -0.25$ nA.

dard enthalpy, ΔS° is the standard entropy, and T is the temperature.) The chains are entropically favored, because there are more possible conformers for an *n*-membered chain compared to an *n*-membered ring. Therefore, the rings must be energetically favored, because otherwise they would not exist at all in equilibrium. The ring closure of a chain therefore has a negative ΔH° and a negative ΔS°. With increasing temperature, the ΔH° term remains approximately constant, whereas the $T\Delta S^\circ$ term strongly increases and makes ΔG° for the ring closure reaction more positive. Since ΔG° is related to the equilibrium constant K^+ via $\Delta G^\circ = -RT\ln K^+$, a more positive ΔG° means that the equilibrium is shifted towards the chains with increasing temperature. In simpler terms, one can argue that the ring closure is an exothermic reaction, for which the equilibrium is shifted to the side of the reactant (i.e., the chain) with increasing temperature, according to the Le Châtelier–Braun principle. In conclusion, the optimum temperature for ring formation is just high enough to reach the regime of thermodynamic control, but not higher, because this reduces the ring yield.

Effective molarity

The concept of the effective molarity (EM) has been introduced for homogeneous (i.e., gas phase or solution) cyclization reactions as a measure for the preference of the intramolecular ring formation over the intermolecular chain growth.[48,49] To our knowledge, this concept has not yet been applied to surface reactions. For kinetic reaction control, the EM is defined as the ratio of the rate constant for the intramolecular over that for the intermolecular reaction k_{intra}/k_{inter}, whereas for thermodynamic control it is the ratio of the corresponding equilibrium constants K_{intra}/K_{inter} (*cf.* Scheme 1).[49]

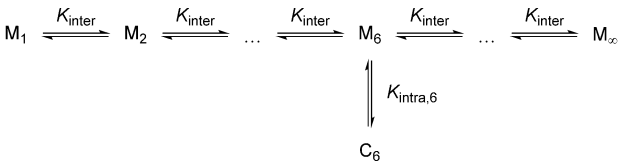

Scheme 1. Reaction Scheme of the equilibrium between the open-chain *i*-mers M_i (equilibrium constant K_{inter}) and the cyclic hexamer C_6 (intramolecular equilibrium constant $K_{intra,6}$).

For on-surface kinetic reaction control, it is not possible to determine the rate constants by real-time STM monitoring, because the reactions are too fast compared to the temporal resolution of the STM experiment. However, the post-reaction product composition can be analyzed with STM and be used to obtain the EM as the ratio of the rate constants. For this, we assume that each addition of a monomer unit to an existing chain corresponds to the intermolecular reaction taking place with the rate constant k_{inter}, whereas each ring closure of an open chain takes place with k_{intra}. For instance, the effective molarity for the cyclic hexamer $EM_6 = k_{intra,6}/k_{inter}$ (where $k_{intra,6}$ is the rate constant for the cyclization of a hexamer chain) can be calculated by dividing the number of cyclic hexamers (which is proportional to $k_{intra,6}$) by the total number of monomers minus the number of rings and chains (to take into account that formation of an oligomer takes one addition reaction less than the total number of monomers). The resulting values for the kinetic EM_6 are plotted as a function of the coverage in Figure 10b; the corresponding data are listed in Table S1 in the Supporting Information.

In the case of thermodynamic control, the determination of the equilibrium constants is in principle also possible by STM-based post-reaction product analysis. The equilibrium EM for a cyclic *i*-mer is defined as $EM_i = K_{intra,i}/K_{inter}$ with the equilibrium constant between an open chain M_i and the cyclic *i*-mer C_i according to $K_{intra,i} = [C_i]/[M_i]$. K_{inter} is the equilibrium constant for the intermolecular model reaction between monofunctional reactants.[50] In our case, this corresponds to the equilibrium constants between chains of different lengths, as shown in Scheme 1. While the concentration of cyclic hexamers can easily be obtained from the STM images by counting, this is not as trivial for the concentration of the corresponding hexamer chains, because the chain lengths are more difficult to measure. Furthermore, only a very small fraction of the chains are hexamers. Thus, a reasonably accurate determination of $K_{intra,i}$ from our experiments is not possible. Additionally, the value for K_{inter} cannot be obtained from the given experiments but would have to be known from literature data.

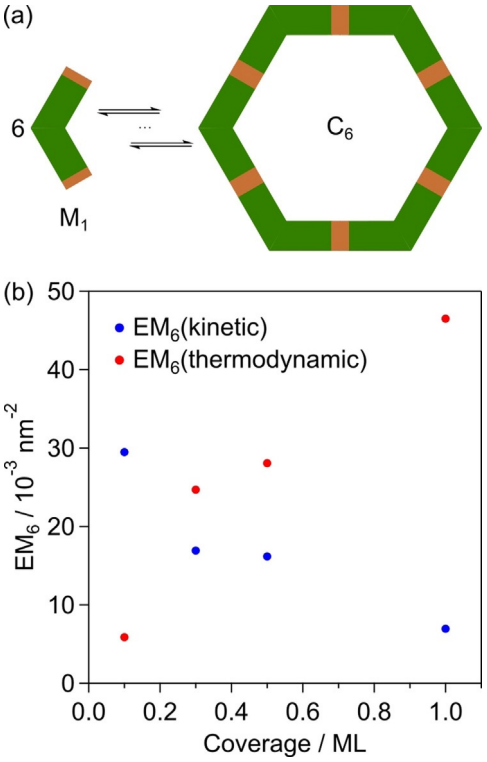

Figure 10. (a) Scheme illustrating the preferred formation of a cyclic hexamer C_6 from six monomers M_1 with two identical functionalities. (b) EM_6 values as a function of the coverage under kinetic reaction control for the four samples shown in Figure 2 and under thermodynamic reaction control as a function of the coverage for the four samples shown in Figure 3.

However, we observe the strong preference of cyclic hexamers over all other ring sizes. This preferential formation of one ring size is known in solution chemistry as self-assembly macrocyclization[51] (which is not to be confused with the self-assembly on surfaces). As illustrated in Figure 10a, six monomers M_1 with two identical functionalities preferably form a cyclic hexamer C_6. The oligomerization proceeds successively starting from a single monomer M_1, which is in equilibrium to chains of different lengths M_i with the intermolecular equilibrium constant K_{inter} (Scheme 1). Only one macrocycle, here the hexamer C_6, is strongly preferred so that it can be formed from the open-chain hexamer M_6 with the respective intramolecular equilibrium constant $K_{intra,6}$. Under the assumption that K_{inter} is independent of the chain length, the concentration of the cyclic *i*-mer can be calculated by $[C_i] = EM_i x^i$, with x being the fraction of reacted end groups in the acyclic fraction of the product mixture.[50] This x can be determined by counting the number of chains and taking into account the total number of monomers (see Table S2 in the Supporting Information). The resulting thermodynamic EM_6 values are shown in Figure 10b. Comparison reveals that the kinetic EM decreases with increasing coverage, while the thermodynamic EM shows the opposite trend. The coverage-dependence of the EM is unexpected and requires interpretation. Both the kinetic and thermodynamic EM are exclusively composed of constants and thus should not depend on the coverage. Nevertheless, this behavior can be understood on a qualitative level. The increase of the thermodynamic EM towards higher coverages means that macrocyclization is overly favored in the high-coverage range. This can be explained by the formation of islands of the cyclic hexamer (*cf.* Figure 3e). The hexamers inside these islands are removed from the equilibrium, resulting in an additional equilibrium shift towards the macrocycle side, according to the Le Châtelier–Braun principle. The beginning of this island formation can already be observed for the coverages of 0.3 and 0.5 ML (*cf.* Figure 3c, d). In the case of kinetic control, it must be considered that the concentrations used here are very high compared to typical reactions in solution. At the highest coverage of 1 ML, the reactants completely fill the available space. For a reaction in the three-dimensional liquid phase, this would be equivalent to the complete absence of a solvent. Under these conditions, the mobility and flexibility of the reactants is strongly reduced. As the coverage increases, the ends of longer chains get increasingly immobile compared to monomers, lowering the probability for ring closure relative to that for the addition of monomers to existing chains. The observed substantial deviations from the expected ideal behavior show that the applicability of the EM concept to on-surface chemistry is limited due to substrate and high-concentration effects.

Conclusions

The ring/chain competition in on-surface organometallic oligomerization was studied in the regimes of kinetic and thermodynamic reaction control using STM and MC simulations. At room temperature, the oligomerization is kinetically controlled and results mainly in the formation of the entropically favored chains, which are formed with a higher statistical probability and thus with higher rates, as was confirmed by MC simulations. Rings prevail at higher temperatures, where the oligomerization is thermodynamically controlled and thus the energetically most stable product is preferentially formed. The ring/chain ratio is coverage-dependent, with higher coverages resulting in lower ring yields both in the experiment and the simulations. This observation can be explained by the different orders of the reactions competing in the dynamic equilibrium: With increasing coverage, the rate of the second-order chain growth increases faster than that of the first-order ring closure. The ring/chain equilibrium is also temperature-dependent and responds to increasing temperatures with lower ring yields, in line with the exothermic nature of the ring formation. Hence, there is a temperature optimum for the ring formation: It is sufficiently high to reach the regime of thermodynamic control, but otherwise as low as possible. Differences to macrocyclization in solution, as revealed by effective molarity considerations, are attributed to the 2D confinement, the preference of certain adsorption sites, and the high concentrations typically used in on-surface synthesis.

Experimental and Computational Details

The experiments were performed in an ultrahigh vacuum (UHV) system (base pressure 2×10^{-10} mbar) equipped with a SPECS Aarhus 150 variable-temperature STM, a SPECS Phoibos 150 electron energy analyzer, and a monochromatized Al Kα X-ray source (SPECS XR 50M, FOCUS 500). STM images were obtained with an electrochemically etched W tip at 100 K in constant current mode and processed with WSxM 5.0 Develop 8.5.[52] All voltages refer to the sample. Moderate filtering (Gaussian smooth, background subtraction) was applied for noise reduction. The Cu(111) single crystal (purity 99.9999%, roughness <0.01 μm, orientation accuracy $<0.1^\circ$, from MaTecK, Germany) was prepared by iterated sputtering with Ar^+ ions (1 keV, 12 μA, 30 min) and annealing (800 K, 10 min). Sample temperatures were measured with a thermocouple directly mounted to the Cu(111) crystal. DBAz (purity >98.0%) was purchased from TCI and deposited on the Cu(111) surface using a custom-built low-temperature Knudsen cell evaporator cooled to 195 K.

The simulations were performed on a rhombic fragment of the triangular lattice with linear size L equal to 200 adsorption sites. To eliminate edge effects, periodic boundary conditions in both directions were imposed. Intermolecular interactions were limited to nearest-neighbor sites on the lattice. The conventional MC method in the canonical ensemble with Metropolis sampling[46,47] was used as follows. In the first step, N molecules were randomly distributed on the surface and the temperature T was fixed. Next, a molecule was picked up at random and its potential energy U_0 was calculated by reckoning the interactions with neighboring molecules. Each of these interactions contributed with ε to U_0. The selected molecule was then moved to a new random position on the lattice and rotated by a multiple of ±60 degrees. If the insertion therein was successful, the potential energy in the new position U_n was obtained using the same procedure as for U_0; otherwise the simulation started from the beginning. To accept the new configuration, the probability factor $p = \min[1, \exp(-\Delta U/kT)]$, where $\Delta U = U_n - U_0$ and k is the Boltzmann factor, was calculated and compared with a

randomly generated number $r \in (0,1)$. If $r < p$, the new configuration was accepted, otherwise the molecule was left in the original (old) position. The above sequence, which constitutes one MC step, was repeated $N \times 10^6$ times to obtain the snapshots and statistics. The average values reported herein were taken over ten independent system replicas using 1% of the final MC steps of each simulation run. Energies and temperatures of our model are expressed in units of ε and $|\varepsilon|/k$, respectively. The surface coverage in the MC simulations was defined as the average number of molecular segments per lattice site, i.e., $2NL^{-2}$. The simulations were performed using 1000, 2000, 4000 and 8000 molecules, which corresponds to the MC surface coverages equal to 0.05, 0.1, 0.2 and 0.4, respectively. Note that the coverages in experiment and simulation have no direct correspondence. Comparison is only meaningful on a qualitative level (e.g., low vs. high coverage). The temperatures in the simulation have the same ratio (T_{high}/T_{low}) as in the experiment, while the absolute temperatures cannot be compared, because the temperature in the simulation is defined with respect to the arbitrary basic energy unit ε. Although we applied Metropolis sampling, which is aimed at reproducing Boltzmann statistics, i.e., the equilibrium case, metastable states can be trapped by immediate cooling directly after the first MC step. This procedure is equivalent to kinetic reaction control in the experiment.

Supporting Information available: X-ray photoelectron spectra, additional STM images, additional MC simulations, data for the effective molarity considerations.

Acknowledgements

Financial support by the Deutsche Forschungsgemeinschaft (DFG, German Research Foundation) through project number 223848855-SFB 1083 and GO1812/2-1 is gratefully acknowledged. Q.F. thanks the Alexander von Humboldt Foundation for a fellowship for postdoctoral researchers. We thank Florian Fillsack, Johannes Glowatzki und Nicole Trebel for support during the measurements.

Conflict of interest

The authors declare no conflict of interest.

Keywords: chain structures · macrocycles · metal–organic frameworks · polymerization · surface chemistry

[1] H. Jacobson, W. H. Stockmayer, *J. Chem. Phys.* **1950**, *18*, 1600 – 1606.
[2] M. Gordon, W. B. Temple, *Makromol. Chem.* **1972**, *152*, 277 – 289.
[3] X.-F. Yuan, A. J. Masters, C. V. Nicholas, C. Booth, *Makromol. Chem.* **1988**, *189*, 823 – 832.
[4] T. Josse, J. De Winter, P. Gerbaux, O. Coulembier, *Angew. Chem. Int. Ed.* **2016**, *55*, 13944 – 13958; *Angew. Chem.* **2016**, *128*, 14150 – 14164.
[5] Q. Fan, C. Wang, Y. Han, J. Zhu, J. Kuttner, G. Hilt, J. M. Gottfried, *ACS Nano* **2014**, *8*, 709 – 718.
[6] Q. Fan, T. Wang, J. Dai, J. Kuttner, G. Hilt, J. M. Gottfried, J. Zhu, *ACS Nano* **2017**, *11*, 5070 – 5079.
[7] Q. Fan, C. Wang, Y. Han, J. Zhu, W. Hieringer, J. Kuttner, G. Hilt, J. M. Gottfried, *Angew. Chem. Int. Ed.* **2013**, *52*, 4668 – 4672; *Angew. Chem.* **2013**, *125*, 4766 – 4770.
[8] Q. Fan, J. Dai, T. Wang, J. Kuttner, G. Hilt, J. M. Gottfried, J. Zhu, *ACS Nano* **2016**, *10*, 3747 – 3754.
[9] C. K. Krug, Q. Fan, F. Fillsack, J. Glowatzki, N. Trebel, L. J. Heuplick, T. Koehler, J. M. Gottfried, *Chem. Commun.* **2018**, *54*, 9741 – 9744.
[10] P. J. Flory, J. A. Semlyen, *J. Am. Chem. Soc.* **1966**, *88*, 3209 – 3212.
[11] G. Franc, A. Gourdon, *Phys. Chem. Chem. Phys.* **2011**, *13*, 14283 – 14292.
[12] J. Méndez, M. F. López, J. A. Martín-Gago, *Chem. Soc. Rev.* **2011**, *40*, 4578 – 4590.
[13] R. Lindner, A. Kühnle, *ChemPhysChem* **2015**, *16*, 1582 – 1592.
[14] Q. Fan, J. M. Gottfried, J. Zhu, *Acc. Chem. Res.* **2015**, *48*, 2484 – 2494.
[15] P. A. Held, H. Fuchs, A. Studer, *Chem. Eur. J.* **2017**, *23*, 5874 – 5892.
[16] M. Lackinger, *Chem. Commun.* **2017**, *53*, 7872 – 7885.
[17] Q. Sun, R. Zhang, J. Qiu, R. Liu, W. Xu, *Adv. Mater.* **2018**, *30*, 1705630.
[18] Q. Shen, H.-Y. Gao, H. Fuchs, *Nano Today* **2017**, *13*, 77 – 96.
[19] M. Chen, J. Shang, Y. Wang, K. Wu, J. Kuttner, G. Hilt, W. Hieringer, J. M. Gottfried, *ACS Nano* **2017**, *11*, 134 – 143.
[20] A. Gourdon in *On-Surface Synthesis*, Springer, Switzerland, **2016**.
[21] D. G. de Oteyza, C. Rogero in *On-Surface Synthesis II*, Springer, Switzerland, **2018**.
[22] S. Clair, D. G. de Oteyza, *Chem. Rev.* **2019**, *119*, 4717 – 4776.
[23] Q. Fan, J. Zhu, J. M. Gottfried in *Organometallic Structures and Intermediates in Surface Ullmann Coupling* (Ed.: K. Wandelt), Elsevier, Oxford, **2018**, pp. 343 – 353.
[24] J. Liu, T. Dienel, J. Liu, O. Groening, J. Cai, X. Feng, K. Müllen, P. Ruffieux, R. Fasel, *J. Phys. Chem. C* **2016**, *120*, 17588 – 17593.
[25] A. Shiotari, T. Nakae, K. Iwata, S. Mori, T. Okujima, H. Uno, H. Sakaguchi, Y. Sugimoto, *Nat. Commun.* **2017**, *8*, 16089.
[26] J. Hieulle, E. Carbonell-Sanromà, M. Vilas-Varela, A. Garcia-Lekue, E. Guitián, D. Peña, J. I. Pascual, *Nano Lett.* **2018**, *18*, 418 – 423.
[27] S. Mishra, M. Krzeszewski, C. A. Pignedoli, P. Ruffieux, R. Fasel, D. T. Gryko, *Nat. Commun.* **2018**, *9*, 1714.
[28] S. Mishra, T. G. Lohr, C. A. Pignedoli, J. Liu, R. Berger, J. I. Urgel, K. Müllen, X. Feng, P. Ruffieux, R. Fasel, *ACS Nano* **2018**, *12*, 11917 – 11927.
[29] D. Cui, M. Ebrahimi, J. M. Macleod, F. Rosei, *Nano Lett.* **2018**, *18*, 7570 – 7575.
[30] M. Liu, M. Liu, Z. Zha, J. Pan, X. Qiu, T. Li, J. Wang, Y. Zheng, D. Zhong, *J. Phys. Chem. C* **2018**, *122*, 9586 – 9592.
[31] H. Xin, X. Gao, *ChemPlusChem* **2017**, *82*, 945 – 956.
[32] Q. Sun, I. C.-Y. Hou, K. Eimre, C. A. Pignedoli, P. Ruffieux, A. Narita, R. Fasel, *Chem. Commun.* **2019**, *55*, 13466 – 13469.
[33] Q. Fan, D. Martin-Jimenez, D. Ebeling, C. K. Krug, L. Brechmann, C. Kohlmeyer, G. Hilt, W. Hieringer, A. Schirmeisen, J. M. Gottfried, *J. Am. Chem. Soc.* **2019**, *141*, 17713 – 17720.
[34] B. P. Klein, N. J. van der Heijden, S. R. Kachel, M. Franke, C. K. Krug, K. K. Greulich, L. Ruppenthal, P. Müller, P. Rosenow, S. Parhizkar, F. C. Bocquet, M. Schmid, W. Hieringer, R. J. Maurer, R. Tonner, C. Kumpf, I. Swart, J. M. Gottfried, *Phys. Rev. X* **2019**, *9*, 011030.
[35] X. Yang, F. Rominger, M. Mastalerz, *Angew. Chem. Int. Ed.* **2019**, *58*, 17577 – 17582; *Angew. Chem.* **2019**, *131*, 17741 – 17746.
[36] P. Y. Huang, C. S. Ruiz-Vargas, A. M. van der Zande, W. S. Whitney, M. P. Levendorf, J. W. Kevek, S. Garg, J. S. Alden, C. J. Hustedt, Y. Zhu, J. Park, P. L. McEuen, D. A. Muller, *Nature* **2011**, *469*, 389 – 392.
[37] F. Banhart, J. Kotakoski, A. V. Krasheninnikov, *ACS Nano* **2011**, *5*, 26 – 41.
[38] J.-C. Charlier, *Acc. Chem. Res.* **2002**, *35*, 1063 – 1069.
[39] K. Suenaga, H. Wakabayashi, M. Koshino, Y. Sato, K. Urita, S. Iijima, *Nat. Nanotechnol.* **2007**, *2*, 358 – 360.
[40] H. Walch, R. Gutzler, T. Sirtl, G. Eder, M. Lackinger, *J. Phys. Chem. C* **2010**, *114*, 12604 – 12609.
[41] M. Bieri, M.-T. Nguyen, O. Gröning, J. Cai, M. Treier, K. Aït-Mansour, P. Ruffieux, C. A. Pignedoli, D. Passerone, M. Kastler, K. Müllen, R. Fasel, *J. Am. Chem. Soc.* **2010**, *132*, 16669 – 16676.
[42] M. Di Giovannantonio, M. Tomellini, J. Lipton-Duffin, G. Galeotti, M. Ebrahimi, A. Cossaro, A. Verdini, N. Kharche, V. Meunier, G. Vasseur, Y. Fagot-Revurat, D. F. Perepichka, F. Rosei, G. Contini, *J. Am. Chem. Soc.* **2016**, *138*, 16696 – 16702.
[43] M. I. Page, W. P. Jencks, *Proc. Natl. Acad. Sci. USA* **1971**, *68*, 1678 – 1683.
[44] C.-X. Wang, J.-L. Chen, C.-H. Shu, K.-J. Shi, P.-N. Liu, *Phys. Chem. Chem. Phys.* **2019**, *21*, 13222 – 13229.
[45] J. Dai, Q. Fan, T. Wang, J. Kuttner, G. Hilt, J. M. Gottfried, J. Zhu, *Phys. Chem. Chem. Phys.* **2016**, *18*, 20627 – 20634.
[46] D. Nieckarz, P. Szabelski, *Chem. Commun.* **2014**, *50*, 6843 – 6845.
[47] P. Szabelski, W. Rżysko, D. Nieckarz, *J. Phys. Chem. C* **2016**, *120*, 13139 – 13147.

[48] R. Cacciapaglia, S. D. Stefano, L. Mandolini, *Acc. Chem. Res.* **2004**, *37*, 113 – 122.
[49] S. Di Stefano, L. Mandolini, *Phys. Chem. Chem. Phys.* **2019**, *21*, 955 – 987.
[50] G. Ercolani, L. Mandolini, P. Mencarelli, S. Roelens, *J. Am. Chem. Soc.* **1993**, *115*, 3901 – 3908.
[51] G. Ercolani, *J. Phys. Chem. B* **1998**, *102*, 5699 – 5703.
[52] I. Horcas, R. Fernández, J. M. Gómez-Rodríguez, J. Colchero, J. Gómez-Herrero, A. M. Baro, *Rev. Sci. Instrum.* **2007**, *78*, 013705.

Manuscript received: January 28, 2020
Accepted manuscript online: February 7, 2020
Version of record online: June 5, 2020

